



CHORUS

This is the accepted manuscript made available via CHORUS. The article has been published as:

Drumhead surface states and topological nodal-line fermions in TlTaSe_2

Guang Bian, Tay-Rong Chang, Hao Zheng, Saavanth Velury, Su-Yang Xu, Titus Neupert, Ching-Kai Chiu, Shin-Ming Huang, Daniel S. Sanchez, Ilya Belopolski, Nasser Alidoust, Peng-Jen Chen, Guoqing Chang, Arun Bansil, Horng-Tay Jeng, Hsin Lin, and M. Zahid Hasan

Phys. Rev. B **93**, 121113 — Published 28 March 2016

DOI: [10.1103/PhysRevB.93.121113](https://doi.org/10.1103/PhysRevB.93.121113)

Drumhead Surface States and Topological Nodal-Line Fermions in TlTaSe₂

Guang Bian*,¹ Tay-Rong Chang*^{†,2,1} Hao Zheng*,¹ Saavanth Velury,³ Su-Yang Xu,¹
Titus Neupert,^{1,4} Ching-Kai Chiu,⁵ Shin-Ming Huang,^{6,7} Daniel S. Sanchez,¹
Ilya Belopolski,¹ Nasser Alidoust,¹ Peng-Jen Chen,^{8,9,10} Guoqing Chang,^{6,7}
Arun Bansil,¹¹ Horng-Tay Jeng,^{2,10} Hsin Lin^{‡,6,7} and M. Zahid Hasan^{§1}

¹*Laboratory for Topological Quantum Matter and Spectroscopy (B7),*

Department of Physics, Princeton University, Princeton, New Jersey 08544, USA

²*Department of Physics, National Tsing Hua University, Hsinchu 30013, Taiwan*

³*Department of Physics, University of California, Berkeley, California 94720, USA*

⁴*Princeton Center for Theoretical Science,*

Princeton University, Princeton, New Jersey 08544, USA

⁵*Condensed Matter Theory Center, Department of Physics,*

University of Maryland, College Park, Maryland 20742-4111

⁶*Centre for Advanced 2D Materials and Graphene Research Centre*

National University of Singapore, 6 Science Drive 2, Singapore 117546

⁷*Department of Physics, National University of Singapore, 2 Science Drive 3, Singapore 117542*

⁸*Department of Physics, National Taiwan University, Taipei 10617, Taiwan*

⁹*Nano Science and Technology Program,*

Taiwan International Graduate Program, Academia Sinica, Taipei 11529,

Taiwan and National Taiwan University, Taipei 10617, Taiwan

¹⁰*Institute of Physics, Academia Sinica, Taipei 11529, Taiwan*

¹¹*Department of Physics, Northeastern University, Boston, Massachusetts 02115, USA*

* These authors contributed equally to this work.

† g943318@phys.nthu.edu.tw

‡ nilnish@gmail.com

§ mzhasan@princeton.edu

Abstract

A topological nodal-line semimetal is a new state of matter with one-dimensional bulk nodal lines and two-dimensional “drumhead” surface bands. Based on first-principles calculations and an effective $\mathbf{k} \cdot \mathbf{p}$ model, we theoretically propose the existence of topological nodal-line fermions in the ternary transition-metal chalcogenide TiTaSe_2 . The noncentrosymmetric structure and strong spin-orbit coupling give rise to spinful nodal-line bulk states which are protected by a mirror reflection symmetry of this compound. This is remarkably distinguished from other proposed nodal-line semimetals such as $\text{Cu}_3\text{NPb}(\text{Zn})$ in which the nodal line exist only in the limit of vanishing spin-orbit coupling and thus is not as robust. In addition, we show that the drumhead surface states in TiTaSe_2 , which are associated with the topological nodal lines, exhibit an unconventional chiral spin texture and an exotic Lifshitz transition as a consequence of the linkage among multiple drumhead surface-state pockets.

PACS numbers: 73.20.-r, 73.20.At, 73.22.-f, 75.70.Tj

Recently the experimental discoveries of three-dimensional (3D) topological Dirac semimetals and Weyl semimetals¹⁻²¹ have stimulated enormous research interest in topological semimetals. Topological semimetallic (TS) materials are characterized by robust bulk band degeneracies and the associated topological boundary states. In the 3D TS materials, the band degeneracies can be either zero dimensional (0D) discrete nodal points or one dimensional (1D) continuous nodal lines. Materials that host these exotic band structures exhibit unique properties and hold promise for device applications. One prominent example of TS materials with 0D band crossing points are Weyl semimetals. The nodal points of Weyl semimetals carry non-zero chiral charges and are connected by the Fermi arc surface states. They have been experimentally realized in transition metal monpnictides such as TaAs¹¹⁻¹⁵. The topological nodal-line semimetals with 1D band degeneracies are distinct in three aspects compared to the Weyl semimetal: (1) the bulk fermi surface is 1D and 0D in nodal-line semimetals and Weyl semimetals, respectively; (2) the density of states (DOS) of low-energy bulk excitations is proportional to $(E - E_f)^2$ and $|E - E_f|$ in nodal-line and Weyl semimetals, respectively; (3) The nodal lines are accompanied by “drumhead”-like surface states while Weyl nodal points are connected by 1D Fermi arc surface states²²⁻³². The unique properties of nodal-line semimetals offer a playground for studying novel physics arising from correlations between the massless quasiparticles. For example, interaction-induced instabilities that have been broadly discussed for Weyl semimetals should be more likely occurring in nodal-line states due to the higher density of states at the Fermi energy. In addition, the torus-shaped Fermi-surface of a doped nodal line semimetal can lead to unusual transport characteristics.

To this date, there have been several theoretical proposals for a material realization of topological nodal-line semimetals³³⁻³⁷. All these works predict nodal-line bulk states and drumhead surface states. However, the stability of nodal lines in the works requires the absence of spin-orbit coupling (SOC). With the inclusion of SOC, each nodal line is gapped due to the interaction between spin components. In real materials SOC, on the other hand, is ubiquitous, therefore it is important to study nodal-line semimetals under the condition of nonvanishing SOC. Generally, spinful nodal lines are unstable, which can be seen from a simple codimension analysis²⁵. In order to have robust nodal lines in the presence of SOC, an extra crystalline symmetry is needed to protect them. In this work, we report, based on first-principles calculations, the existence of spinful topological nodal lines in the ternary transition-metal chalcogenide TiTaSe_2 . The nodal lines are 0.22 eV below the Fermi level and protected by a mirror reflection symmetry of the space group. The topological

nodal-line state in TlTaSe_2 is in the class $A+R$ ($p = 2$) of symmetry-protected semimetals^{24,26} and is connected with spin-polarized drumhead surface modes. We also demonstrate an exotic Lifshitz transition as a consequence of the linkage among multiple drumhead surface-state pockets. Our results establish TlTaSe_2 a promising material for studying nodal-line physics.

TlTaSe_2 , shown in Fig. 1(a), crystallizes in a hexagonal lattice in which the unit cell consists of one Tl, one Ta and two Se atoms and each atom resides on a hexagonal layer. The stacking sequence of these atomic planes within the unit cell is Tl-Se-Ta-Se: B-A-B-A (A, B and C, here, refer to the three high-symmetry spots on a hexagonal lattice). In other words, the Tl layer intercalates between adjacent TaSe_2 layers with Tl atoms aligned with Ta atoms in the vertical direction. The structure is non-centrosymmetric and belongs to the space group $P\bar{6}m2$ (187). The lattice is reflection-symmetric with respect to both the Ta plane and the Tl plane. This reflection symmetry plays a key role in protecting the topological nodal lines, as discussed later on. Figure 1(b) shows the bulk and (001)-projected surface Brillouin zones where the A, H and L points are high symmetry points on the $k_z = \pi$ plane, a mirror plane of the bulk Brillouin zone. The calculated band structure of TlTaSe_2 without and with the inclusion of SOC is shown in Fig. 1(c). Around the H point, a hole pocket derived from Ta- $5d_{xy/x^2-y^2}$ orbitals crosses an electron pocket from Tl- $6p_{x,y}$ orbitals, taking the plane parallel to the Ta atomic plane as the x - y plane. All these atomic orbitals are invariant under the mirror reflection R_z with respect to the Tl atomic plane. A zoom-in view of band structure around H is plotted in Fig. 1(d). In the case without SOC, the conduction and valence bands belong to different representations of the space group, A' and A'' for electron and hole bands, respectively. The intersection of the two bands is, therefore, protected by the crystalline symmetry, forming a spinless nodal ring on the mirror plane $k_z = \pi$. Upon turning on SOC, each band splits into two spin-polarized branches since the system lacks space inversion symmetry. The spin splitting results in an accidental band touching of Ta and Tl bands at H and three band crossings. Only the band crossing 0.22 eV below the Fermi level remains gapless while the other two are gapped. A detailed analysis on the symmetry, orbital composition and spin texture of the bands around H is presented in Fig. 2(a). The bands are mainly comprised of Ta- $5d_{xy/x^2-y^2}$ and Tl- $6p_{x,y}$ states which are mostly confined the Ta and Tl atomic planes, respectively. The spin of these states is primarily oriented along z as indicated in Fig. 2(a). At the gapless crossing point, the two branches have opposite mirror parity eigenvalues. Therefore, this band crossing is protected by the mirror symmetry, forming a pair of nodal rings

on the mirror plane $k_z = \pi$, one around H and the other around H'. To visualize the nodal rings, we plot the iso-energy contour at $E = -0.18$ eV, shown in Fig. 2(b). The energy is slightly off the nodal-line energy (-0.22 eV), which creates a toroidal Fermi surface enclosing nodal lines. Indeed, we can find two rings surrounding H and H' points on $k_z = \pi$ plane. At the center of the bulk Brillouin zone there is a spherical Fermi surface which is the hole pocket around Γ mainly derived from the Ta- $5d_{3z^2-r^2}$ orbitals.

To further illustrate the mechanism of mirror-symmetry protection on the nodal rings, we develop an effective $\mathbf{k} \cdot \mathbf{p}$ description taking the four relevant bands around H into account, see³⁸ for details. The band structure from the effective Hamiltonian is plotted in Fig. 2(c), which is in good agreement with the first-principles result and thus confirms the symmetry protection of the nodal lines. Considering the crystalline symmetry of TlTaSe₂, the nodal line at H is classified as the time-reversal breaking class A+R which admits a bulk integer topological classification for Fermi surfaces of codimension 2, i.e., lines ($p = 2 \text{ in}^{24}$), indicating that there can exist multiple bulk nodal lines in this system. We note that the entire system preserves time-reversal symmetry (\mathbb{T}) but breaks space-inversion symmetry (\mathbb{P}), so the effective Hamiltonian at H lacks the composite symmetry \mathbb{TP} (and \mathbb{T} as well), which puts the nodal lines of TlTaSe₂ in a distinct class other than those reported in^{34,36}. The nodal lines of TlTaSe₂ are characterized by a topological quantum number n^+ , which is given by the difference in the number of occupied bands with mirror reflection eigenvalue $+i$ inside and outside the nodal line. In the case at hand, $n^+ = +1$ for the nodal line at H in the $k_z = \pi$ plane as shown in Fig. 2(c). To deduce topological surface states, n^+ can be related to a topological invariant given by the Berry phase,

$$\mathcal{P}(k_x, k_y) = -i \sum_{E_j < E_f} \int_{-\pi}^{\pi} \langle u_j(\mathbf{k}) | \partial_{k_z} | u_j(\mathbf{k}) \rangle dk_z, \quad (1)$$

where the sum is over all occupied Bloch eigenstates $|u_j(\mathbf{k})\rangle$ ³⁹. According to⁴⁰, the Berry phase $\mathcal{P}(k_x, k_y)$ (quantized in units of π) is related to the charge at the end of the one-dimensional system obtained by fixing k_x and k_y , therefore the non-zero Berry phase guarantees the existence of the topological surface state and the topological invariant of the nodal ring can be viewed as the variation of the Berry phase, $\Delta\mathcal{P} = \pm\pi$, across the ring. In other words, each nodal ring with $\Delta\mathcal{P} = \pm\pi$ must connect to a single drumhead surface state. Figure 2(d) shows the jump of the Berry phase of TlTaSe₂ across the ring, indicating the topological character of the nodal ring. The Berry phase is defined modulo 2π due to the fact that large gauge transformations of the wave

functions can change it by 2π . If $\mathcal{P}(k_x, k_y) = \pi \bmod 2\pi$, there exist an odd number of drumhead surface states at k_x, k_y in the surface Brillouin zone³⁹.

H and H' points are time-reversal partners in k space. Considering spinful nodal lines in TlTaSe_2 , the mirror operator \mathbb{M} can be written as $i\sigma_z$ and the time reversal operator \mathbb{T} as $K\sigma_y$, where K is the complex conjugate operator and $\sigma_{y,z}$ are Pauli matrices acting on spin. \mathbb{M} and \mathbb{T} commute with each other and, therefore, the nodal lines at H and H' have the same topological mirror invariant. We also perform a band structure calculation in which the Ta atom is slightly moved in the vertical direction and, thus, the mirror reflection symmetry is broken. In this case all of the four branches around H are found to belong to the same S_2 representation of the reduced space group and a gap opening is allowed at every crossing point of these branches, as shown in Fig. 2(e). Therefore, the nodal line in this case is gapped by mirror-symmetry-breaking perturbations. In other words, the nodal rings in TlTaSe_2 are indeed protected by the mirror reflection symmetry.

Next we study the evolution of the nodal lines as SOC varies. The nodal-line band structure at various SOC is plotted in Fig. 3(a). As shown in the above discussion, without SOC there is a spinless nodal line around H. Once SOC is turned on, each band splits into two spin branches with opposite mirror parity eigenvalues and the spinless crossing line is, consequently, split into four spinful crossing lines. However, among these four crossing lines only two are robust under the protection of mirror reflection symmetry. In this case they are the crossings between bands b1 and b4 and between b2 and b3, because the mirror parity of b2 and b4 is $+i$ and that of b1 and b3 is $-i$. So there are two nodal rings around H arising from the two symmetry-protected band crossings. The crossings between b1 and b3 and between b2 and b4 are gapped. The gap size at the topmost b1-b3 crossing is very small, but it can be evidently seen in Fig. 2(a) and explained by our effective Hamiltonian as shown in Fig. 2(c). As SOC increases, bands b2 and b3 are gradually pulled apart from each other and with $\text{SOC} = 1$ in the scale relative to the real SOC of the material the two bands barely touch. For even larger SOC, e.g., $\text{SOC} = 1.2$, the two bands separate and, as a result, the nodal ring associated with these two bands disappears. Therefore only one nodal ring is left when SOC is beyond the critical value 1. In Fig. 3(b), we plot the energy difference between the top of band b2 and the bottom of band b3 as a function of SOC. Varying SOC, we have three different phases of nodal lines, namely, spinless nodal line, double nodal line, and single nodal line. A detailed discussion on the drumhead surface states in the three phases can be found in the online supplementary materials³⁸.

In order to illustrate connection of drumhead surface states with the bulk nodal lines, the surface electronic structure is constructed using a first-principles-derived tight-binding model Hamiltonian in a slab. The projected (001)-bulk band structure along $\bar{\Gamma} - \bar{K} - \bar{M}$ direction is plotted in Fig. 4(a) where the nodal line is clearly seen. The surface can be terminated with either a Se layer or a Tl layer, because the bonding between Se and Tl atoms is much weaker than that between Se and Ta atoms. The surface band structure corresponding to the two possible terminations is shown in Figs. 4(b) and 4(c). In both cases, the drumhead band disperses outwards from the line nodes, consistent with the calculated nonzero Berry phase outside the ring shown in Fig. 2(d). We note that it is not guaranteed that the drumhead surface states must appear within the bulk band gap, because the system lacks chiral symmetry³¹. The topology-derived surface states can, in principle, entirely merge into bulk band continuum (but continue to exist). Therefore some of the topological surface states in the gap are just accidental and their dispersion is highly surface sensitive. It is the connection of the topological drumhead band with the nodal ring that is protected by the topology, and the location of drumhead states (inside or outside the ring) is determined by the Berry phase. In the case of Se termination, the surface band disperses outwards with respect to \bar{K} from the nodal line, grazes outwards at the edge of the bulk band below the nodal line, and merges into the bulk band region, as marked by the arrows in Fig. 4b. This can be also seen in the iso-energy band contour at $E = -0.25$ eV (slightly below the energy of the nodal line, -0.22 eV), shown in Fig. 4(d). The drumhead surface states overlap with the bulk nodal rings and there is no other surface state at this energy. On the other hand, the surface band structure on the Tl-terminated surface is dramatically different. Along $\bar{\Gamma} - \bar{K}$ direction, starting from the nodal point, the surface band grazes outwards at the edge of the upper bulk Dirac cone and merges into the bulk band. Along $\bar{K} - \bar{M}$ direction, the drumhead surface band $SS1$ disperses into the bulk band gap. Within the gap there exists a second surface band $SS2$ which joins the drumhead band at \bar{M} forming a Kramers pair. The spin polarization of the two surface bands is shown in Fig. 4(e). The two surface bands possess opposite spin polarizations. The overall surface band structure and spin texture resemble those of the Dirac surface states of topological insulators^{41,42}. The drumhead surface band has no spin degeneracy and it arises from the band inversion of two spinful bulk bands (b1 and b4). Figure 4(f) shows the iso-energy band contours of Tl-terminated surface at three different energies [indicated by dotted lines in Fig. 4(e)]. At $E = -0.25$ eV, slightly below the energy of the nodal rings, two surface bands form a human-eye-shaped contour, lying in between two nodal-ring bulk

pockets at \bar{K} and \bar{K}' . The spin texture is unconventional in the sense that as moving along either surface band clockwise, the spin orientation rotate in counterclockwise direction (see³⁸ for details). The spin orientation is not always in the tangential direction of the Fermi surface contour, which is distinct from the spin-momentum-locked texture of Dirac surface states in conventional topological insulators⁴¹⁻⁴³. At the energy of the nodal rings ($E = -0.22$ eV), the eye-shaped contour connects to the nodal rings and, as energy moves further up, the corners of the eyes open and the drumhead surface band $SS1$ transforms into a large closed contour surrounding $\bar{\Gamma}$. This topological change in the band contour is known as Lifshitz transition in the electronic structure. The Lifshitz transition discussed here is special in two aspects: (1) the transition and the associate saddle-point singularity happen in spin-polarized 2D surface bands; (2) the transition relies on a linkage of multiple small pockets around \bar{M} to form a giant pocket surrounding $\bar{\Gamma}$. This exotic linkage of 2D surface bands give rise to a divergence in the DOS at the von Hove singularities, like the case of topological crystalline insulators and high- T_c superconductors⁴⁴⁻⁴⁷. Shifting chemical potential to the Lifshitz transition energy in TlTaSe₂ by means of chemical doping or electrical gating can potentially trigger interaction-induced instabilities such as unconventional superconductivity⁴⁶ or spin/charge density waves at the surface.

In summary, topological nodal-line semimetals form a distinct class of topological materials beyond topological insulators and Weyl semimetals. In this work we propose theoretically that TlTaSe₂, a ternary transition-metal chalcogenide, is a promising candidate for material realization of topological nodal-line semimetals. Unlike previous proposed materials, the nodal lines in TlTaSe₂ are robust even with the inclusion of SOC as long as the mirror reflection symmetry with respect to the Ta atomic plane is not broken. The nodal line is 0.22 eV below the Fermi level and, thus, accessible to the conventional ARPES measurements. Through systematic surface simulations, we show the unique spinful drumhead surface states on Se-terminated surface and, even more interestingly, find that Tl-terminated surface of TlTaSe₂ features a Lifshitz transition as a consequence of the exotic linkage of multiple drumhead surface-state pockets. In light of these novel properties of the electronic band structure of TlTaSe₂, we establish an ideal material platform for studying unique physics, including possible electronic correlation effect, of topological nodal-line semimetals.

I. ACKNOWLEDGEMENTS

T.R.C. acknowledges visiting scientist support from Princeton University. We thank Chuang-Han Hsu for technical assistance in the theoretical calculations. We thank Chen Fang and Andreas P. Schnyder for discussions. The work at Princeton University was supported by the by U.S. DOE/BES under DE-FG-02-05ER46200. The work at Northeastern University was supported by the US Department of Energy (DOE), Office of Science, Basic Energy Sciences grant number DE-FG02-07ER46352, and benefited from Northeastern University's Advanced Scientific Computation Center (ASCC) and the NERSC supercomputing center through DOE grant number DE-AC02-05CH11231. H.L. acknowledges the Singapore National Research Foundation for the support under NRF Award No. NRF-NRFF2013-03. T.R.C. and H.T.J. were supported by the National Science Council, Taiwan. H.T.J. also thanks the National Center for High-Performance Computing, Computer and Information Network Center National Taiwan University, and National Center for Theoretical Sciences, Taiwan, for technical support.

-
- ¹ H. Weyl, *Z. Phys.* **56**, 330 (1929).
 - ² G. E. Volovik, *The Universe in a Helium Droplet* (Oxford University Press, 2003).
 - ³ C. Herring, *Phys. Rev.* **52**, 365 (1937).
 - ⁴ F. Wilczek, *Phys. Today* **51**, 11 (1998).
 - ⁵ L. Balents, *Physics* **4**, 36 (2011).
 - ⁶ M. Z. Hasan, S.-Y. Xu, and G. Bian, *Phys. Scr.* **T164**, 014001 (2015).
 - ⁷ X. Wan, A. M. Turner, A. Vishwanath, and S. Y. Savrasov, *Phys. Rev. B* **83**, 205101 (2011).
 - ⁸ A. A. Burkov and L. Balents, *Phys. Rev. Lett.* **107**, 127205 (2011).
 - ⁹ G. Xu, H. Weng, Z. Wang, X. Dai, and Z. Fang, *Phys. Rev. Lett.* **107**, 186806 (2011).
 - ¹⁰ B. Singh, A. Sharma, H. Lin, M. Z. Hasan, R. Prasad, and A. Bansil, *Phys. Rev. B* **86**, 115208 (2012).
 - ¹¹ S.-M. Huang, S.-Y. Xu, I. Belopolski, C.-C. Lee, G. Chang, B. Wang, N. Alidoust, G. Bian, M. Neupane, C. Zhang, S. Jia, A. Bansil, H. Lin, and M. Z. Hasan, *Nat. Commun.* **6**:7373 (2015).
 - ¹² S.-Y. Xu, I. Belopolski, N. Alidoust, M. Neupane, G. Bian, C. Zhang, R. Sankar, G. Chang, Z. Yuan, C.-C. Lee, S.-M. Huang, H. Zheng, J. Ma, D. S. Sanchez, B. Wang, A. Bansil, F. Chou, P. P. Shibayev, H. Lin, S. Jia, and M. Z. Hasan, *Science* **349**, 613 (2015).

- ¹³ H. Weng, C. Fang, Z. Fang, A. Bernevig, and X. Dai, *Phys. Rev. X* **5**, 011029 (2015).
- ¹⁴ B. Q. Lv, H. Weng, B. B. Fu, X. P. Wang, H. Miao, J. Ma, P. Richard, X. C. Huang, L. X. Zhao, G. F. Chen, Z. Fang, X. Dai, T. Qian, and H. Ding, *Phys. Rev. X* **5**, 031013 (2015).
- ¹⁵ H. Zheng, S.-Y. Xu, G. Bian, C. Guo, G. Chang, D. S. Sanchez, I. Belopolski, C.-C. Lee, S.-M. Huang, X. Zhang, R. Sankar, N. Alidoust, T.-R. Chang, F. Wu, T. Neupert, F. Chou, H.-T. Jeng, N. Yao, A. Bansil, S. Jia, H. Lin, and M. Z. Hasan, *ACS Nano* **10**, 1378 (2016).
- ¹⁶ S.-Y. Xu, C. Liu, S. K. Kushwaha, R. Sankar, J. W. Krizan, I. Belopolski, M. Neupane, G. Bian, N. Alidoust, T.-R. Chang, H.-T. Jeng, C.-Y. Huang, W.-F. Tsai, H. Lin, P. P. Shibayev, F.-C. Chou, R. J. Cava and M. Z. Hasan, *Science* **347**, 294 (2015).
- ¹⁷ B.-J. Yang and N. Nagaosa, *Nat. Commun.* **5**, 4898 (2014).
- ¹⁸ Z. Wang, H. Weng, Q. Wu, X. Dai, and Z. Fang, *Phys. Rev. B* **88**, 125427 (2013).
- ¹⁹ M. Neupane, S.-Y. Xu, R. Sankar, N. Alidoust, G. Bian, C. Liu, I. Belopolski, T.-R. Chang, H.-T. Jeng, H. Lin, A. Bansil, F. Chou, and M. Zahid Hasan, *Nat. Commun.* **5**, 3786 (2014).
- ²⁰ S. Borisenko, Q. Gibson, D. Evtushinsky, V. Zabolotnyy, B. Büchner, and R. J. Cava, *Phys. Rev. Lett.* **113**, 027603 (2014).
- ²¹ Z. K. Liu, B. Zhou, Y. Zhang, Z. J. Wang, H. Weng, D. Prabhakaran, S.-K. Mo, Z. X. Shen, Z. Fang, X. Dai, Z. Hussain, and Y. L. Chen, *Science* **343**, 864 (2014).
- ²² A. A. Burkov, M. D. Hook, and L. Balents, *Phys. Rev. B* **84** 235126 (2011).
- ²³ M. Phillips and V. Aji, *Phys. Rev. B* **90**, 115111 (2014).
- ²⁴ C. Chiu and A. P. Schnyder, *Phy. Rev. B* **90**, 205136 (2014).
- ²⁵ C. Fang, Y. Chen, H.-Y. Kee, and L. Fu, *Phy. Rev. B* **92**, 081201 (2015).
- ²⁶ G. Bian, T.-R. Chang, R. Sankar, S.-Y. Xu, H. Zheng, T. Neupert, C.-K. Chiu, S.-M. Huang, G. Chang, I. Belopolski, D. S. Sanchez, M. Neupane, N. Alidoust, C. Liu, B. Wang, H.-T. Jeng, A. Bansil, F. Chou, H. Lin, and M. Z. Hasan, *Nat. Commun.* **7**, 10556 (2016).
- ²⁷ S. A. Yang, H. Pan, and F. Zhang, *Phys. Rev. Lett.* **113**, 046401 (2014).
- ²⁸ J. W. McClure, *Phys. Rev.* **108**, 612 (1957).
- ²⁹ G. P. Mikitik and Yu. V. Sharlai, *Phy. Rev. B* **73**, 235112 (2006).
- ³⁰ T. T. Heikkilä and G. E. Volovik, *New J. Phys.* **17**, 093019 (2015).
- ³¹ A. Schnyder and S. Ryu, *Phy. Rev. B* **84**, 060504 (2011).
- ³² D. Gosálbez-Martínez, I. Souza, and. Vanderbilt, *Phys. Rev. B* **92**, 085138 (2015).

- ³³ L. S. Xie, L. M. Schoop, E. M. Seibel, Q. D. Gibson, W. Xie, and R. J. Cava, *APL Materials* **3**, 083602 (2015).
- ³⁴ R. Yu, H. Weng, Z. Fang, X. Dai, and X. Hu, *Phys. Rev. Lett.* **115**, 036807 (2015).
- ³⁵ M. Zeng, C. Fang, G. Chang, Y.-A. Chen, T. Hsieh, A. Bansil, H. Lin, and L. Fu, arXiv:1504.03492 (2015).
- ³⁶ Y. Kim, B. J. Wieder, C. L. Kane, and A. M. Rappe, *Phys. Rev. Lett.* **115**, 036806 (2015).
- ³⁷ H. Weng, Y. Liang, Q. Xu, R. Yu, Z. Fang, X. Dai, and Y. Kawazoe, *Phys. Rev. B* **92**, 045108 (2015).
- ³⁸ See online supplementary materials.
- ³⁹ Y.-H. Chan, C.-K. Chiu, M. Y. Chou, and A. P. Schnyder, arXiv:1510.02759 (2015).
- ⁴⁰ D. Vanderbilt and R. D. King-Smith, *Phys. Rev. B* **48**, 4442 (1993).
- ⁴¹ M. Z. Hasan and C. L. Kane, *Rev. Mod. Phys.* **82**, 3045 (2010).
- ⁴² X.-L. Qi and S.-C. Zhang, *Rev. Mod. Phys.* **83**, 1057 (2011).
- ⁴³ G. Bian, L. Zhang, Y. Liu, T. Miller, and T.-C. Chiang, *Phys. Rev. Lett.* **108**, 186403 (2012).
- ⁴⁴ Y. Okada, M. Serbyn, H. Lin, D. Walkup, W. Zhou, C. Dhital, M. Neupane, S. Xu, Y. J. Wang, R. Sankar, F. Chou, A. Bansil, M. Z. Hasan, S. D. Wilson, L. Fu, and V. Madhavan, *Science* **341**, 1496 (2013).
- ⁴⁵ J. E. Hirsch and D. J. Scalapino, *Phys. Rev. Lett.* **56**, 2732 (1986).
- ⁴⁶ D. M. King, Z. -X. Shen, D. S. Dessau, D. S. Marshall, C. H. Park, W. E. Spicer, J. L. Peng, Z. Y. Li, and R. L. Greene, *Phys. Rev. Lett.* **73**, 3298 (1994).
- ⁴⁷ C. Liu, T. Kondo, R. M. Fernandes, A. D. Palczewski, E. D. Mun, N. Ni, A. N. Thaler, A. Bostwick, E. Rotenberg, J. Schmalian, S. L. Bud'ko, P. C. Canfield, and A. Kaminski, *Nat. Phys.* **6**, 419 (2010).

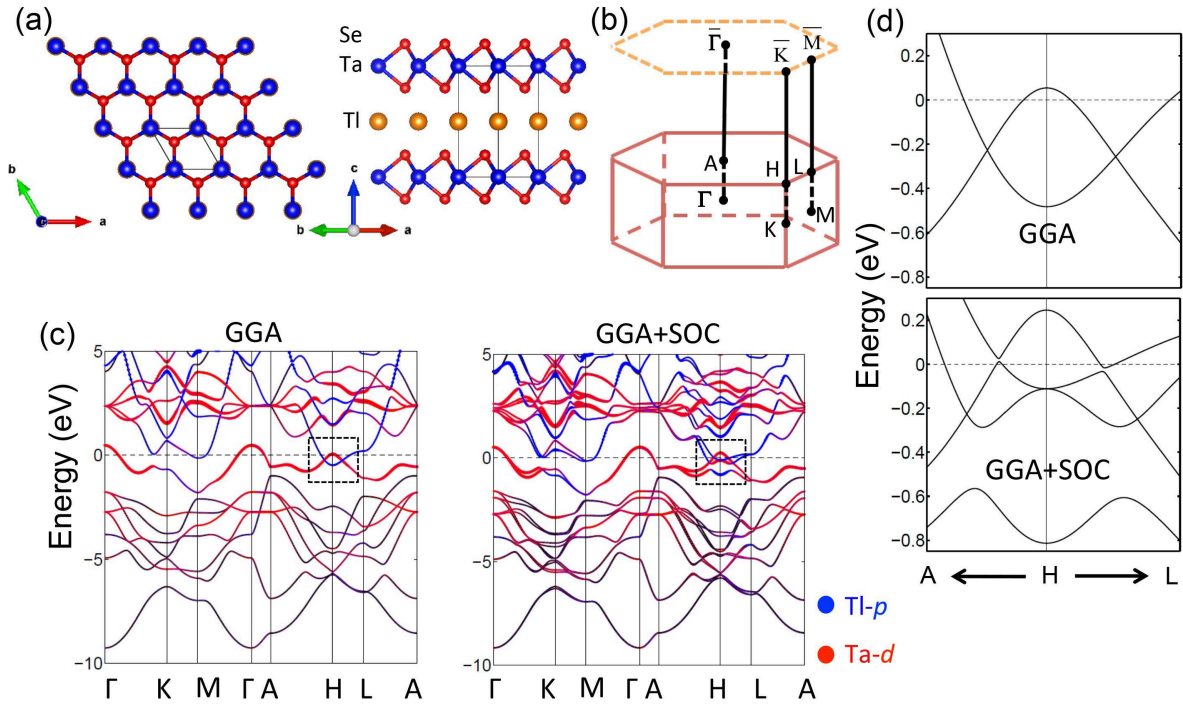


FIG. 1: (color online). (a) Lattice structure of TlTaSe₂: top view (left) and side view (right). (b) Bulk and (001)-projected surface Brillouin zones. (c) Calculated bulk band structure of TlTaSe₂ without (left) and with (right) the inclusion of spin-orbit coupling. The color shows the atomic orbital decomposition. (d) Zoom-in band structure around H point as marked in (c).

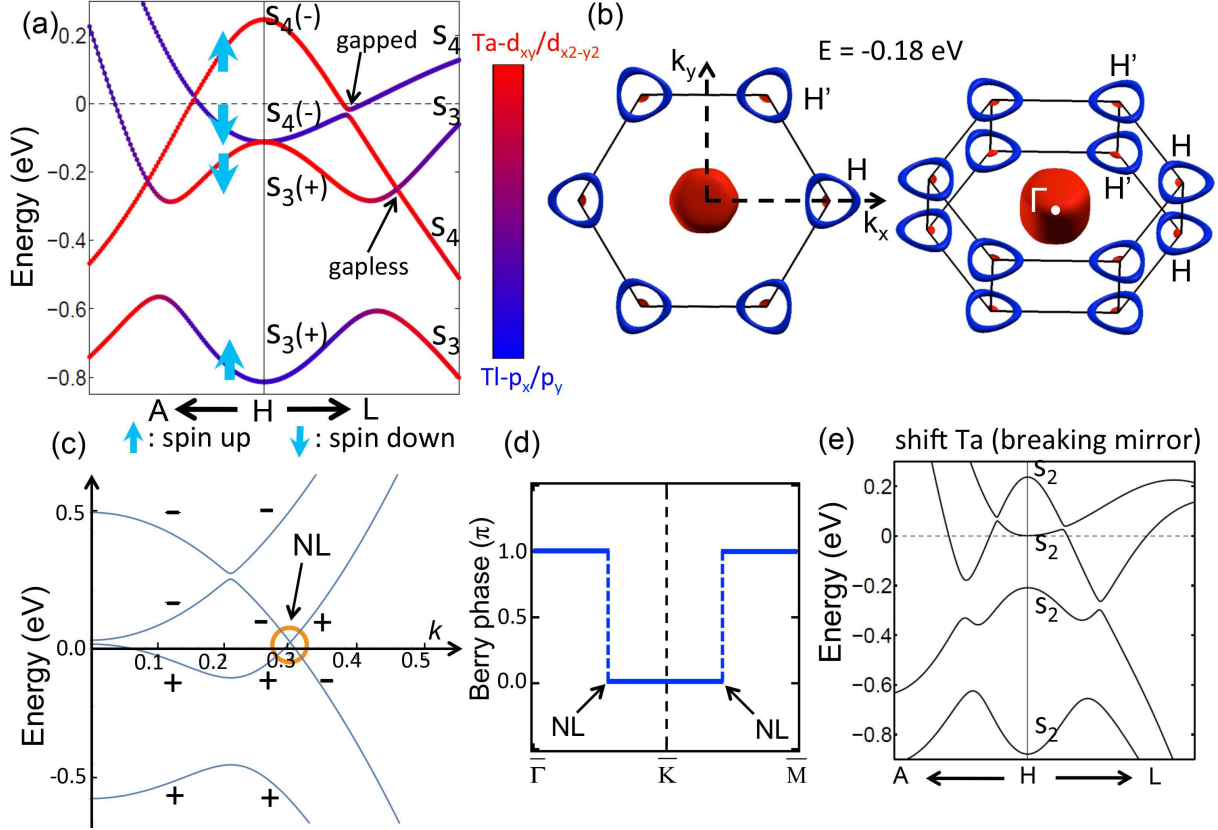


FIG. 2: (color online). (a) Orbital composition, space-group representation and spin polarization of nodal-line (NL) bands in TlTaSe₂. The mirror parity of each band is given in parentheses. (b) Iso-energy bulk-band contour at $E = -0.18$ eV of TlTaSe₂ bulk bands. (c) Band structure of the effective $\mathbf{k} \cdot \mathbf{p}$ model that approximates the low energy bands around the H point for parameters $m_1 = 0.7$, $m_2 = 0.8$, $\mu = 2.2$, $\Delta_{\text{SOC}} = 2.5$. See³⁸ for details. (d) Variation of the Berry phase along high-symmetry lines of the surface Brillouin zone of TlTaSe₂, taking into account the two bands that constitute the nodal ring. \bar{K} is inside the nodal ring whereas $\bar{\Gamma}$ and \bar{M} outside the ring. (e) Calculated bulk band structure of TlTaSe₂ with the Ta atom shifted slightly away from the equilibrium position in the unit cell. The shift breaks the mirror symmetry of the system and reduces the symmetry of the nodal-line states.

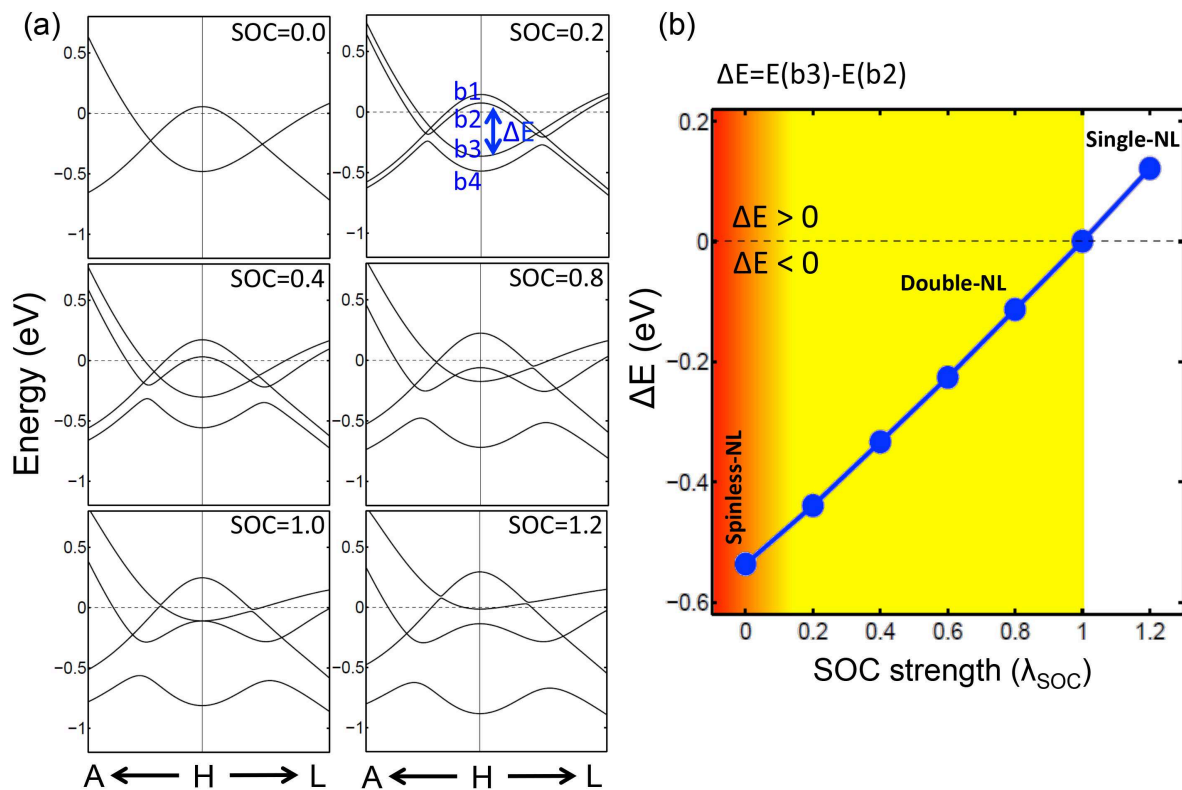


FIG. 3: (color online). (a) The nodal-line band structure of TlTaSe₂ with various SOC (in the scale relative to the SOC of the material). (b) The energy difference between the two bands b2 and b3 as a function of SOC, showing nodal-line phases at different SOC.

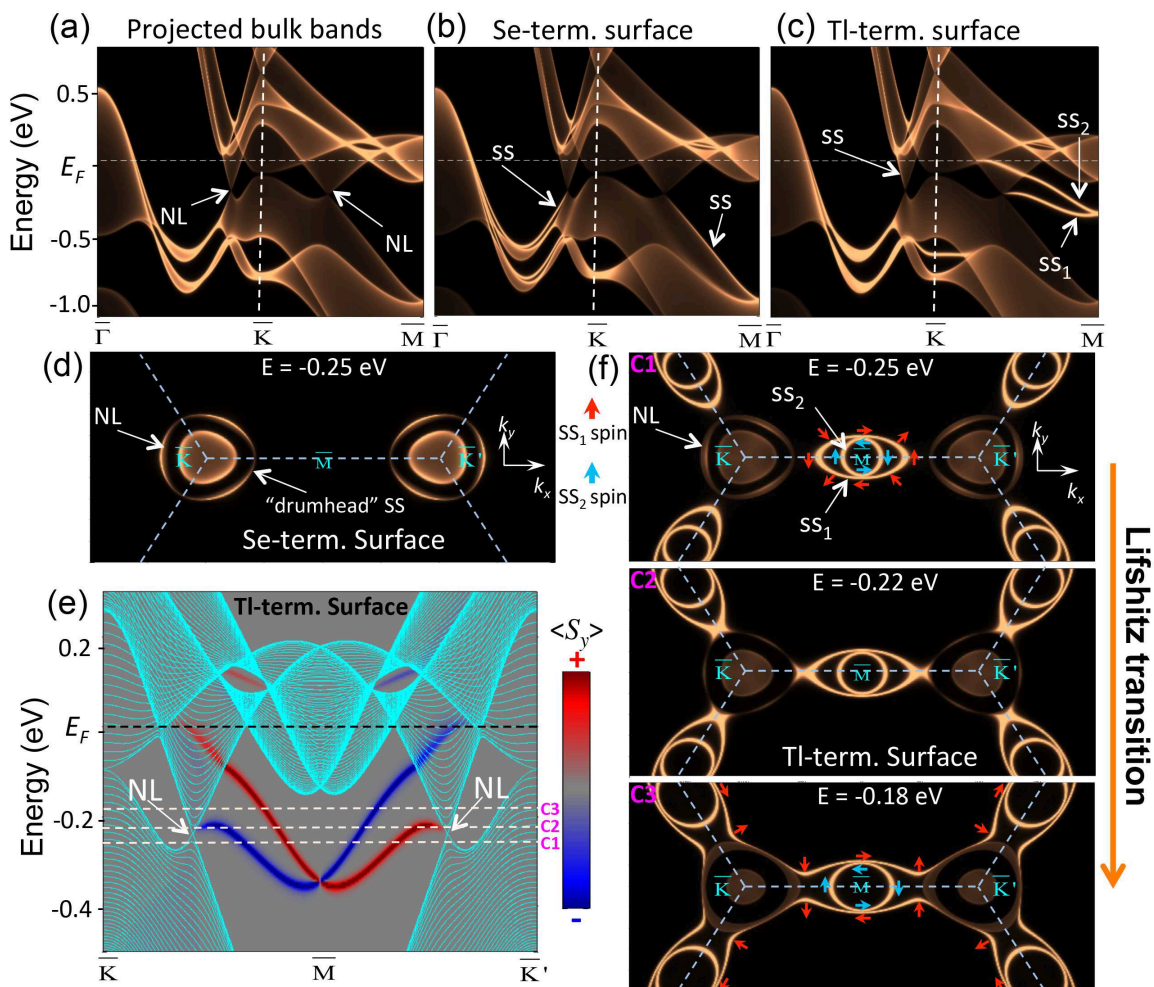


FIG. 4: (color online). (a) (001)-projected bulk bands of TlTaSe_2 . (b) Bulk and surface band structure of Se-terminated surface of TlTaSe_2 . The surface bands are marked by the arrows. (c) Same as (b) but for Tl-terminated surface of TlTaSe_2 . (d) Iso-energy band contour at $E = -0.25$ eV of Se-terminated surface. The drumhead surface states overlap with the bulk nodal rings. (e) The spin polarization of surface bands of Tl-terminated surface. (f) Iso-energy band contour at $E = -0.25$ eV (top), -0.22 eV (middle), and -0.18 eV (bottom) of Tl-terminated surface. The arrows indicate the spin texture of the surface bands.